# Egyptian Journal of Chemistry

http://ejchem.journals.ekb.eg/

# Optical, Structure and Dielectric Properties of Er³⁺ Ions Doped Al-Na-K-Ba Phosphate Glasses

**M.M. Ismail[1*], H. Farouk[2], Lidia Zur[3], Alessandro Chiasera[3], Maurizio Ferrari[3,4], Anna Lukowiak[5], A.Ashery[1], M. A. Salem[1] and I.K.Battisha[1*]**

[1]*National Research Centre, Solid State Physics Department, Physics Research Division,33 El Behooth St., Dokki, Giza, Egypt, (Affiliation ID: 60014618).*

[2] *Al AZHAR University, Physics Department, Faculty of Science, Cairo, Egypt.*

[3]*IFN-CNR CSMFO Lab. and FBK Photonics Unit, Povo, Trento, Italy.*

[4]*Museo Storico della Fisica e Centro Studi e Ricerche "Enrico Fermi", Piazza del Viminale 1, 00184, Roma, Italy.*

[5]*Institute of Low Temperature and Structure Research, PAS, Okolna, 2, 50-422, Wroclaw, Poland.*

**E**r³⁺-doped Na-Al-K-Ba phosphate glasses were prepared by conventional melt quenching technique. The structure was studied using XRD and it showed that all the samples were in amorphous form. Physical properties such as density and refractive index have been measured. While the dielectric studies were carried out using (KEYSIGHT-E4991B) over a wide range of frequency extending from 1 MHz up to 1GHz ($10^6$ up to $10^9$ Hz) at room temperature (RT). The absorbance spectra were measured and The Judd–Ofelt analysis has been carried out, hence the radiative properties of $^4I_{13/2} \rightarrow {}^4I_{15/2}$ transition were obtained. High radiative and experimental lifetime for the Er³⁺ ions has been detected. The experimental lifetime and quantum efficiency found to be decreased with increasing Er³⁺ content. These results obviously indicate that the present glasses may be promising for optical amplifiers as well as laser applications around 1522 nm.

**Keywords:-** Phosphate glass, Erbium, Judd-Ofelt, lifetime, Mc-Cumber, Dielectric properties

## Introduction

Recently, the trivalent erbium (Er³⁺) ions doped different glass matrices have attracted a great deal of attention due to its potential applications in lasers, optical amplifiers and optical sensors. Er³⁺ ion shows unique emissions around 1500 nm corresponding to $^4I_{13/2} \rightarrow {}^4I_{15/2}$ 4f transition. The mentioned transition attracted attention since it is located in the low-loss window of glass [1, 2]. Moreover, Er³⁺ ion has another important emission around 540 nm corresponds to $^4S_{3/2} \rightarrow {}^4I_{15/2}$ transition which used in green laser applications [3].

In general, the rare-earth ions spectral properties are strongly dependent on the local field around the ion, phonon energies of the host matrix, refractive index and defects in the glass matrix.

Recently, phosphate glasses have received a great deal of attention due to its low non-linear refractive index [4], its high rare earth ions solubility without clustering and the phonon energy of phosphate glasses (~1200 cm⁻¹), makes it almost insensitive to up-conversion phenomena [5].

The main purpose of this work is to prepare multi-component phosphate glasses incorporated with various concentrations of Er³⁺ ion. The physical, structure, chemical bonding and optical properties of the prepared samples will be studied.

## Experimental

*Glass preparation*

Phosphate glasses with the composition (mol%) of 60% $P_2O_5$ + 8% $Al_2O_3$ + 2% $Na_2O$ + 17% $K_2O$ + (13-x)% BaO + x% $Er_2O_3$ (x= 0.2, 0.75, 1.5 and 3 %) were prepared using conventional melt quenching technique which are symbolic as PANKB0.2Er, PANKB0.75Er, PANKB1.5Er and PANKB3Er.

High purity $P_2O5$, $Al_2O_3$, $Na_2CO_3$, $BaCO_3$, $K_2CO_3$, and $Er(NO_3)_35H_2O$ were used as starting materials to prepare the glasses. A batch of 30 grams of starting materials was thoroughly mixed in an agate mortar and the homogeneous mixture was taken in a Porcelain crucible and kept in an electric furnace at a temperature of 1100⁰C for 2 h. The melt was then poured onto a preheated stainless steel mold at a temperature of 430 ⁰C until the glass solidifies. Then the glass samples were annealed at the same temperature 430 ⁰C for 2 hours to remove thermal strains and stress. After that the samples were allowed to cool to room temperature. Finally, the prepared glasses were cut and polished for optical measurements.

*Characterization techniques*

The density of the samples was determined by Archimede's method with water as an immersion liquid. The refractive indices of these glasses were measured using PTR 46X refractometer at 589 nm with the mono-bromonapthalene as the contact layer between the samples and prism of the refractometer. X-ray diffraction (XRD) patterns for the prepared samples were recorded with a Philips X-ray diffractometer using mono-chromatized $CuK_{\alpha 1}$ radiation of wavelength 1.54056Å from a fixed source operated at 45 kV and 9 mA. FTIR spectra were recorded on a Mattson 5000 FTIR spectrometer in the wavenumber's range between 400 and 1600 $cm^{-1}$ .with a resolution of 1 $cm^{-1}$ . Absorption spectra (300-1650 nm) were measured using a UV/VIS/NIR spectrophotometer Model V-570. The instrument specified by resolution 0.1 nm and wavelength accuracy ±0.3 nm (at a spectral bandwidth of 0.5 nm).

The dielectric properties were measured in a wide range of frequencies between 1 MHz and 1 GHz using network impedance analyzer (KEYSIGHT-E4991B), shown in Fig. 2.2.1.

The samples were inserted between two cupper conducting electrodes of 10mm in diameter forming capacitor. The dielectric properties such

as capacitance (C) and loss tangent (tanδ) can be measured using the mentioned (KEYSIGHT-E4991B). For the present samples, the permittivity (ε') and AC conductivity (σac) were calculated from these parameters at room temperature in the frequency range (106 – 109 Hz) as follows:

$$\varepsilon' \ = \ \frac{Cd}{\varepsilon_o A} \qquad (3)$$

$$\sigma_{ac} \ = \ \omega \varepsilon_o \varepsilon' \tan \delta \qquad (4)$$

Where $\varepsilon_o$ is the permittivity of free space (8.854 x $10^{-12}$ F/m), ω (= 2πf) is the angular frequency of the applied electric field in Hertz, d is the sample thickness and A is the sample surface area.

The photoluminescence spectra and the lifetime measurements were performed by exciting the samples with a diode laser at 514.5 nm. The excitation power was 0.5 mW for all the measurements. The luminescence signal was dispersed by a single grating monochromator with a resolution of 0.5 nm and 2 nm for the emission and excitation spectra, respectively, and was detected using a Hamamatsu photomultiplier and standard lock-in technique .The photoluminescence measurement wavelength range was from 1400 to 1700 nm. The measurements were made on glasses and glasses powder, immediately after glass preparation and all spectra were measured at room temperature.

## Results and Discussion

*Physical properties*

The density of the samples (*ρ),* the average molecular weight (*M_w)* and The $Er^{3+}$ ions concentration *(N)* were calculated as in [6] and all the results were tabulated in Table 1. **A.**

It can be noticed that n is constant while $M_w$ and N are slightly increased by increasing **Er³⁺** content. The *ρ* is almost constant up to 1.5% Er then it starts to increase.

*XRD*

**Fig.1** shows the XRD patterns of PANKB0.2Er, PANKB0.75Er, PANKB1.5Er and PANKB3Er glasses. No diffraction patterns were observed for all the samples and over all the measured range. Those results assume the amorphous nature of our glasses.

*FTIR Spectra*

Fig. 2 shows typical infrared spectra of PANKB0.2Er, PANKB0.75Er PANKB1.5Er and PANKB3Er phosphate glasses in the frequency range between 400 and 1600 $cm^{-1}$. A number of

**Fig. 2.2.1. The wide range frequencies between 1 MHz and 1 GHz using network impedance analyzer (KEYSIGHT-E4991B).**

**TABLE 1. A. The physical properties of PANKB0.2Er, PANKB0.75Er, PANKB1.5Er and PANKB3Er glasses, respectively.**

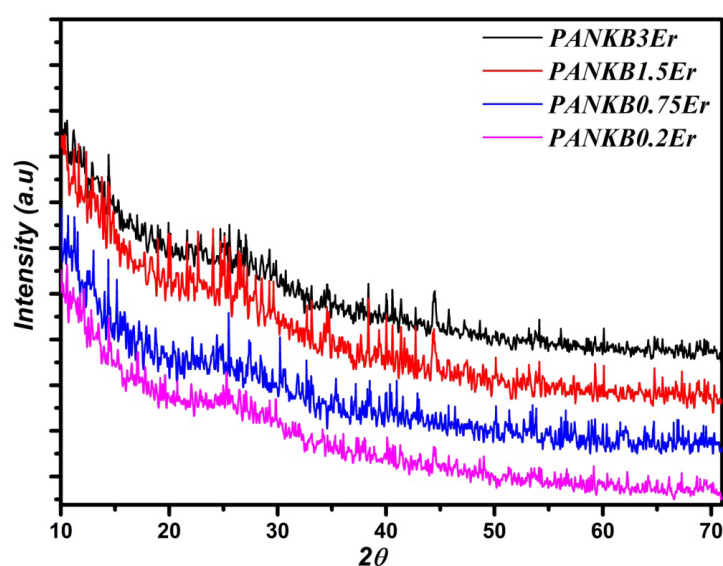| Samples | N | Physical properties | | |
|---------|---|---------------------|---|---|
| | | $\rho(gm/cm^3)$ | $N(\times10^{+20}ions/cm^3)$ | $M_w$ (gm) |
| PANKB0.2Er | 1.65 | 2.76 | 0.508 | 130.97 |
| PANKB0.75Er | 1.65 | 2.75 | 1.879 | 132.23 |
| PANKB1.5Er | 1.65 | 2.75 | 3.705 | 133.95 |
| PANKB3Er | 1.65 | 2.79 | 7.356 | 137.38 |



**Fig.1. The XRD patterns of PANKB0.2Er, PANKB0.75Er, PANKB1.5Er and PANKB3Er, respectively.**

strong characteristics meta-phosphate glass bands can be observed. As seen from Fig. 2, there is a triplet band around 513 cm$^{-1}$, a broad band around 750 cm$^{-1}$, Quartet in the regions 815-1210 cm$^{-1}$ and an intense broad band around 1290 cm$^{-1}$. Infrared spectra seem to be composed of relatively broad absorption bands which could indicate the structural disorder of the various phosphate structural groups.

There is no sufficient evidence for the existence of bands characteristic of P-O-M group, where M is the other cations present in the glass matrix (Al, Na, Ba, K, Er) but we supposed that the stretching band corresponding to P-O-M linkages might locate between 900 and 1165 cm$^{-1}$, but not observable due to overlapping with other bands in that range. A similar idea has been proposed by Xu and Day [7] for Sn-P-O-F glasses.

A comparison of PANKB0.2Er, PANKB0.75Er PANKB1.5Er and PANKB3Er spectra show that all the samples have almost similar FTIR spectra, which may be due to similar composition of the glass matrix except little amount of Er$^{3+}$ ions, which seems to have a low or negligible effect on FTIR absorption spectra. Careful observation of present results reveals a limited variation in the amplitude and frequencies of the bands; this is may be due to the exchange of formation between linear meta-phosphate chain and meta-phosphate rings. From another point of view, the meta-phosphate chains and meta-phosphate rings themselves have different lengths and radius.

*Dielectric measurements*

The dielectric studies provide useful information about applied electric field distribution, charge transportation mechanism inside glasses, chemical bonds and their polarization mechanism.

One of the most important dielectric properties is the complex permittivity which is giving by the following relation:

$$\varepsilon^*(\omega) = \varepsilon'(\omega) + i\varepsilon''(\omega) \quad (1)$$

Where the real part of the complex dielectric constant is called the permittivity ($\varepsilon'$) and the imaginary part is called the dielectric loss ($\varepsilon''$) that originates from the friction of the dipole moments.

Experimentally $\varepsilon'$ can be determined using the following relation:

$$\varepsilon' = \frac{C\,d}{A\,\varepsilon_0} \quad (2)$$

Where $\varepsilon_0$ is the permittivity of free space, C is the capacitance of the measured sample in Farad, A is the cross-sectional area of the sample, d is the thickness of the sample in meter. While $\varepsilon''$ can be determined using the following relation:

$$\varepsilon'' = \varepsilon' \, tan\delta \quad (3)$$

Where *tanδ* is the dissipation factor.

The effect of the increase in the Er3+ ions concentration on the permittivity ε', dielectric loss $\acute{\varepsilon}$, were drawn in Fig. 3 and the AC conductivity, σac, in Fig. 4 for PANKB0.2Er, PANKB0.75Er, PANKB1.5Er and PANKB3Er glasses, respectively. The $\acute{\varepsilon}$, $\acute{\varepsilon}$ and σac were measured over a wide range of frequency extending from 1 MHz up to 1GHz (106 up to 109 Hz) at room temperature (RT). In fact, the dielectric is used to study the charge transport mechanism of the materials. The dielectric studies were carried out using (KEYSIGHT-E4991B). Polished amorphous glasses were placed between two cupper electrodes for such measurements. It can be seen from Fig. 3 that the $\acute{\varepsilon}$ and $\acute{\varepsilon}$ for all samples decreases with increasing frequency. The permittivity decreases within the mentioned frequency range is attributed to the total polarization decrease, i.e. electronic and orientation polarization. Electronic polarization arises from the displacement of electrons relative to nucleus, whereas the orientation of polarization caused from rotation of dipolar molecules or flipping, or ions changing places. While, in this higher frequency range dielectric loss ($\acute{\varepsilon}$) decreases by increasing the frequency consequently starts to increase another time in some samples. The dielectric properties of the studied samples in such high frequency range were investigated under the influence of uniaxial mechanical stress which, is applied in parallel with the measurement direction. The steep increase in ε' by decreasing the frequency (at lower frequency range) supposed to be attributed to the ionic migration which is responsible to the conductivity contribution. It can be seen from the same figure that ε'' show a sufficient decrease by increasing the frequency almost linearly. This is attributed to the fact that the majority of the dielectric loss at lower frequencies is due to the conductivity contribution and/or the space charge polarization.

One can conclude that further increase of the frequency shows a collapsing of the permittivity values for all investigated samples and the ε' became nearly independent on frequency. The
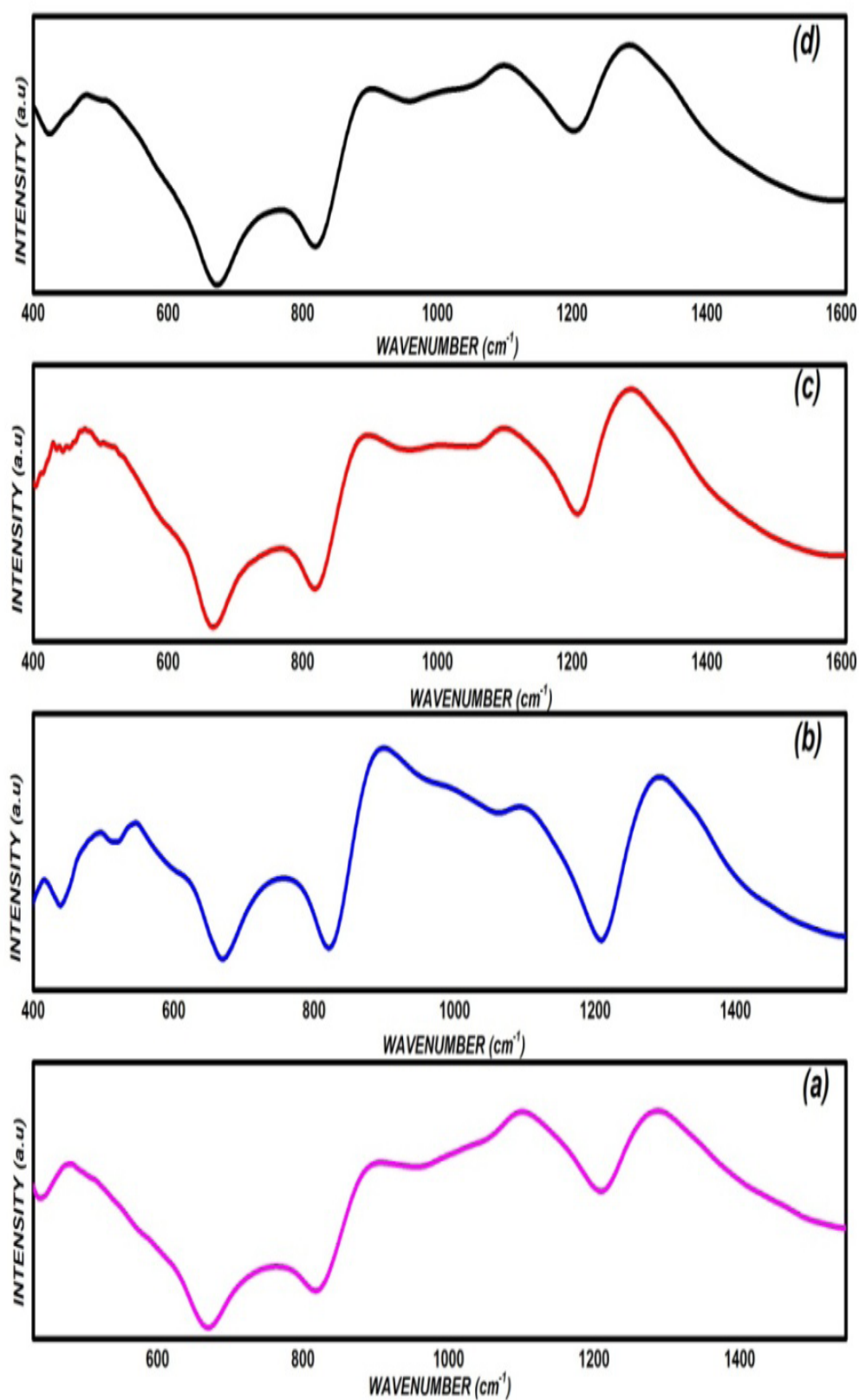
**Fig. 2. The absorbance FTIR spectra for PANKB0.2Er (a), PANKB0.75Er (b), PANKB1.5Er (c), and PANKB3Er (d) glasses extended from 400 up to 1600 cm⁻¹.**

measured permittivity can be attributed to the existence of permanent electrical dipoles in the glass [8] that arise from charged pairs formed by the positively charged metal cations and negatively charged Qn groups. By increasing the frequency, the dipoles can hardly follow the oscillations of the electric field and one can detect the collapsing of the $\acute{\varepsilon}$ and $\acute{\varepsilon}$ values. At high frequency, the dipolar polarization can no longer follow the oscillations of the electric field and the ε' become nearly independent on frequency.

Whereas ε' relatively increases by increasing the Er3+ ions concentration at constant frequency value equal to 1E07 from 0.2 up to 1.5 mol % then it suddenly decreases at 3 mol %. The different behaviors observed for the addition of Er3+ ions concentration is probably due to the appearance of erbium clusters at higher concentration than 1.5 mol %, confirmed by the obtained ρ data in Table 1. A. in this work, which are almost constant up to 1.5% Er3+ ions then it starts to increase at 3 mol % Erbium ions concentration.

By focusing on the A.C conductivity obtained data one can observe from Figure 4 that the A.C. conductivity for all the prepared samples (PANKB0.2Er, PANKB0.75Er, PANKB1.5Er and PANKB3Er) remarkably increased by increasing the frequency in the range between 1E7 MHz and 1E9GHz, obeying the universal power law Aωs [23]. The σac of the samples was calculated using the equation (4) section 2.2. The reason for this obtained result came from free charge carriers alignments towards the electric field and the long range movements, causing a net charge flow through the discussed glasses sample.

In order to highlight on the erbium ions embedded amorphous prepared glasses dependency on the σac at specific 3 constant frequency values (1E6 MHz, 5.0E8 MHz and 1E9 GHz), see Table 1. B., it is observed that σac is a little bit decreases (nearly constant up to 1.5 mol % of Er3+ ions embedded nano-composite prepared samples). Then it can be noted that it has increased with the increase in the erbium ions concentration at 3 mol %. The obtained results may be attributed to the increase in charge carriers due to the appearance of erbium clusters at higher concentration than 1.5 mol %, confirmed by the obtained ρ data in Table 1. A. in this work, where the density are almost constant up to 1.5% Er3+ ions then it starts to increase at 3 mol % Erbium ions concentration.

*Optical properties*

Fig.4 shows absorption coefficient (α) spectra of PANKB0.2Er, PANKB0.75Er, PANKB1.5Er and PANKB3Er glasses in the region ranged from 350 up to 1650 nm. The spectrum consists of 12 bands corresponding to the transitions from the ground state $^4I_{15/2}$ to the various excited states $^4I_{13/2}$, $^4I_{11/2}$, $^4I_{9/2}$, $^4F_{9/2}$, $^4S_{3/2}$, $^2H_{11/2}$, $^4F_{7/2}$, $^4F_{5/2}$, $^4F_{3/2}$, $^2G_{9/2}$, $^4G_{11/2}$ and $^4G_{9/2}+^2K_{15/2}$, respectively. The absorption bands are assigned to the energy levels by comparing with previously reported Er3+glass matrices [9-12].

The spin–orbit (ζ) and electrostatic $F_{(2)}$, $F_{(4)}$, $F_{(6)}$ parameters were calculated using standard least-square fitting approach between calculated energy levels and experimental energy levels using RELEC program [13]. The calculations were made for PANKB0.2Er, PANKB0.75Er, PANKB1.5Er and PANKB3Er glasses and the results are shown in Table.2.

The experimental oscillator strengths $(f_{exp})$ for all the absorption bands of Er3+ ions can be obtained from the absorptivity spectra using (equation 3) [14].

$$f_{exp}(\Psi J \rightarrow \Psi'J') = \frac{mc^2}{\pi e^2}\int \varepsilon(k)dk = 4.318 \times 10^{-9}\int \varepsilon(k)dk \quad (3)$$

where $k$ is the wavenumber ( cm⁻¹), m and e are the mass and the charge of the electron, respectively and c is the speed of light.

According to Judd-Ofelt theory [14, 15] the total oscillator strength can be given by equation (4)

$$f_{calc}(\Psi J \rightarrow \Psi'J') = \frac{8\pi^2 m v_0}{3h(2j+1)n^2}[\chi_{ed}S_{ed}+\chi_{md}S_{md}] \quad (4)$$

Where $S_{md}$ and $S_{ed}$ are the magnetic and electric dipole strengths, $\chi_{ed}=n(n^2+2)^2/9$ and $\chi_{md}=n^3$ are the electric and magnetic Dexter correction factor for the field within a medium of refractive index $n$

$$S_{ed}(\Psi J \rightarrow \Psi'J') = \frac{8\pi^2 mk_0 \chi_{ed}}{3h(2j+1)n^2}\left[\sum_{t=2,4,6}\Omega_t |\langle i||U^t||j\rangle|^2\right] \quad (5)$$

$$S_{md}(\Psi J \rightarrow \Psi'J') = \frac{e^2 h^2 \chi_{md}}{16\pi^2 m^2 c^2}|\langle i||L+2S||j\rangle|^2 \quad (6)$$

Where $\Omega_t$ (t=2, 4, and 6) are Judd-Ofelt intensity parameters, m is the mass of electron, $k_0$ is the wave-number at the centroid of absorption band (cm⁻¹), $2J+1$ is the degeneracy of the originating level of the transition, h is the Plank constant = 6.6261 x 10-27 erg.sec, the $\langle i||U^t||j\rangle$ and $\langle i||L+2S||j\rangle$ are the doubly reduced matrix elements of the tensor operator $U^k$ and $L+gS$
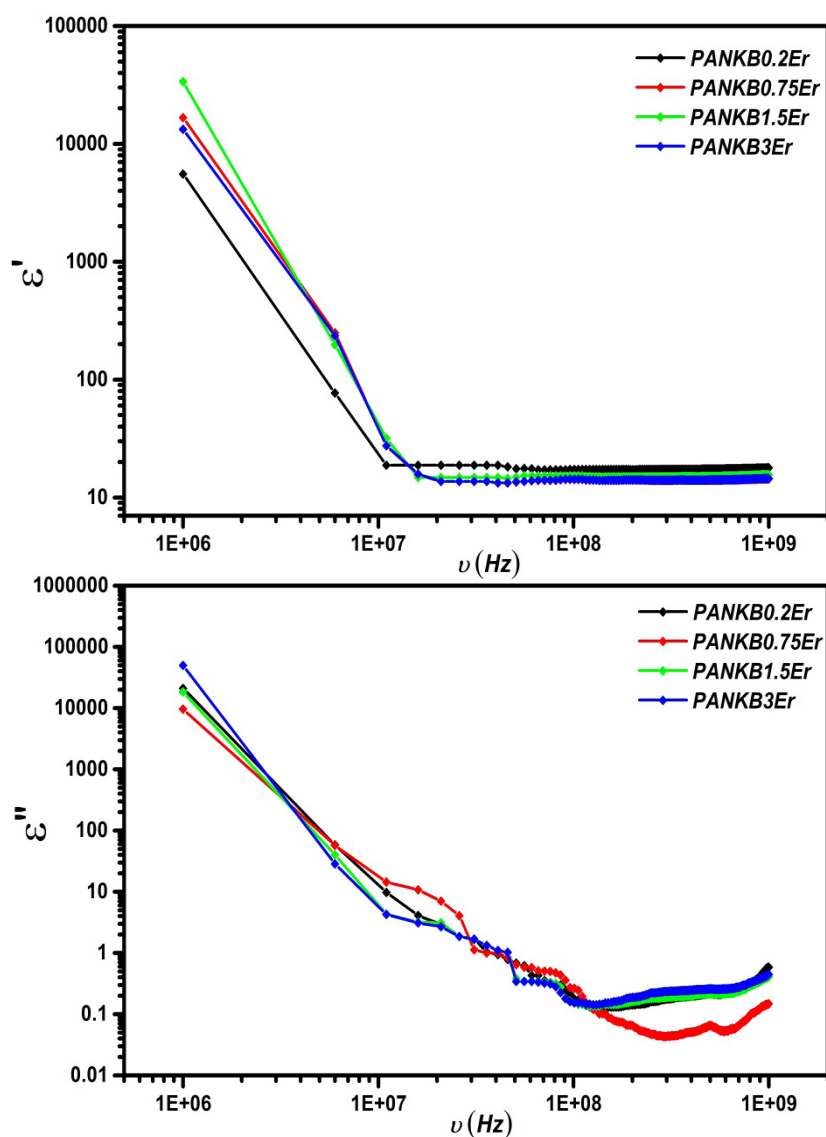
Fig. 3. Frequency dependence of $\varepsilon'$ and $\varepsilon''$ for PANKB0.2Er, PANKB0.75Er, PANKB1.5Er and PANKB3Er glasses.

TABLE 1. (B). The $\sigma_{ac}$ of PANKB0.2Er, PANKB0.75Er, PANKB1.5Er and PANKB3Er glasses, respectively at fixed frequencies; 1E6 MHz, 5.0E8 MHz and 1E9 GHz.

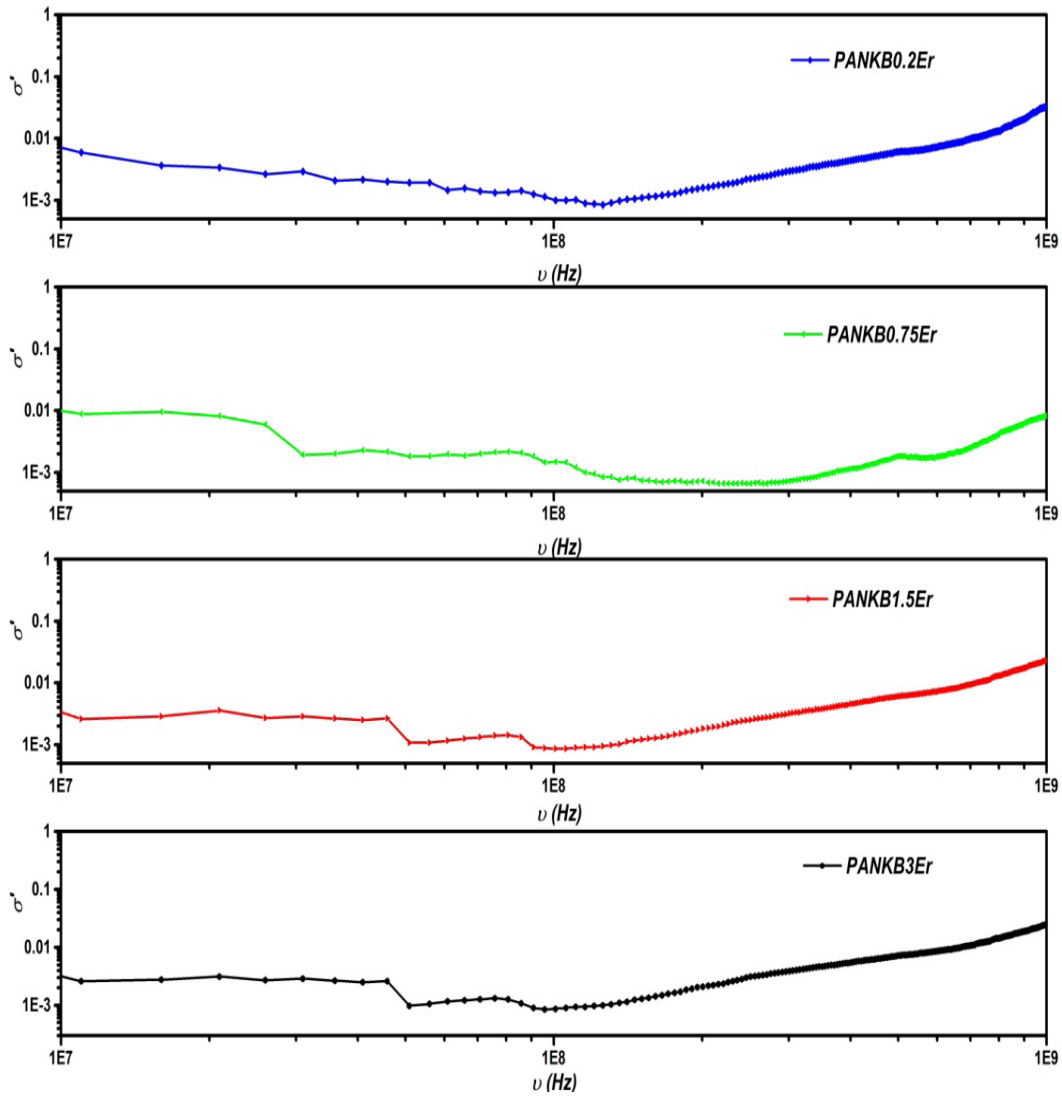| Samples abbreviation | $\sigma_{ac}$ at 1E6 MHz, 5.0E8 MHz and 1E9 GHz. | | |
|---|---|---|---|
| | 1E6 MHz | 5.0E8 MHz | 1E9 GHz |
| PANKB0.2Er | 0.18618 | 0.00609 | 0.03267 |
| PANKB0.75Er | 0.08516 | 0.00183 | 0.00818 |
| PANKB1.5Er | 0.16298 | 0.00603 | 0.0226 |
| PANKB3Er | 0.4442 | 0.00719 | 0.02477 |

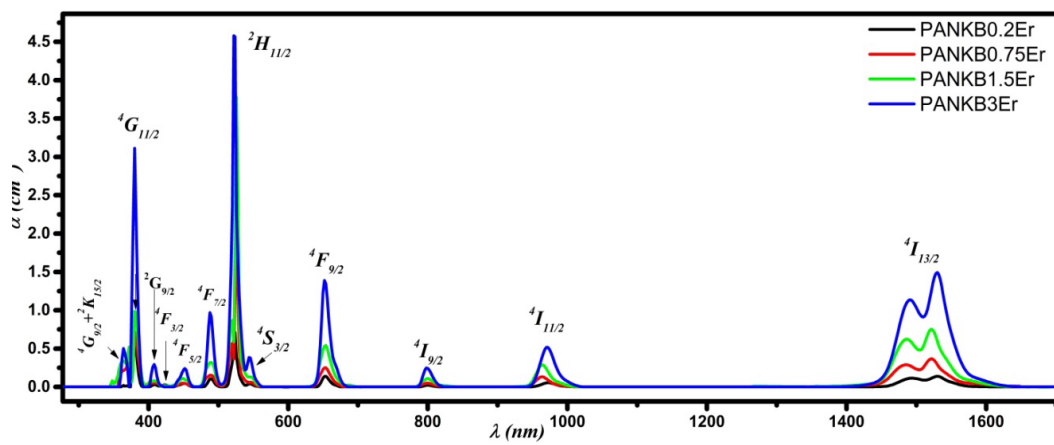**Fig. 4. The σ$_{ac}$ of PANKB0.2Er, PANKB0.75Er, PANKB1.5Er and PANKB3Er, respectively.**



**Fig. 4. The absorption Coefficient spectra PANKB0.2Er, PANKB0.75Er, PANKB1.5Er and PANKB3Er glasses.**

**TABLE 2. F$_{(2)}$, F$_{(4)}$, F$_{(6)}$) and ζ parameters for PANKB0.2Er, PANKB0.75Er, PANKB1.5Er and PANKB3Er glasses**

| Samples | Parameters | | | |
|---|---|---|---|---|
| | F$_{(2}$ | F$_{(4)}$ | F$_{(6)}$ | ζ |
| PANKB0.2Er | 437.4 | 65.7 | 7.1 | 2428.5 |
| PANKB0.75Er | 433.4 | 66.4 | 7.3 | 2433.8 |
| PANKB1.5Er | 432.9 | 66.4 | 7.3 | 2433.3 |
| PANKB3Er | 434.1 | 66.6 | 7.3 | 2417.8 |

respectively, and they have been calculated as in [16, 17] using RELIC program[13].

The intensity parameters, $\Omega_t$ (t=2, 4, and 6) can be calculated using least-square fitting between $f_{calc}$ and $f_{exp}$.

The Judd-Ofelt parameters are sensitive to the glass composition. The value of $\Omega_2$ is pointing to covalent bonding between surrounding ligands and rare earth ions, whereas $\Omega_4$ and $\Omega_6$ parameters are related to the rigidity of the medium [18]. The $\Omega_t$ parameters of PANKB0.2Er, PANKB0.75Er, PANKB1.5Er and PANKB3Er glasses are tabulated in Table.3. It can be seen that the $\Omega_2$ of the prepared glass firstly decreased by increasing Er³⁺ content then starts to increase again. $\Omega_4$ and $\Omega_6$ have minima for PANKB0.75Er sample.

Judd-Ofelt parameters can be used to calculate some important radiative parameters such as:-

The spontaneous emission probability (*A*) of a certain transition is given by the equation (7) [19].

$$A_r(\Psi J \rightarrow \Psi' J') = \frac{64\pi^4 \nu_0^3 e^2}{3h(2j+1)} \left[ \frac{n(n^2+1)^2}{9} S_{ed} + n^3 S_{md} \right] \quad (7)$$

Where $S_{md}$ and $S_{ed}$ are the magnetic and electric dipole strengths respectively which are given by equation 8 and 9

$$S_{md}(\Psi J \rightarrow \Psi' J') = \frac{h^2}{16\pi^2 m^2 c^2} |\langle J\|L+2S\|J'\rangle|^2 \quad (8)$$

$$S_{ed}(\Psi J \rightarrow \Psi' J') = \sum_{k=2,4,6} \Omega_t |\langle J\|U^k\|J'\rangle|^2 \quad (9)$$

The total radiative transition probability $A_t(\Psi J)$ of an excited level is given by the sum of the $A(\Psi J \rightarrow \Psi' J')$ terms calculated over all terminal levels [19].

$$A_t(\Psi J) = \sum A(\Psi J \rightarrow \Psi' J') \quad (10)$$

The fluorescence branching ratio $B_r$ has been determined using

$$B_r = \frac{A(\Psi J \rightarrow \Psi' J')}{A_t(\Psi J)} \quad (11)$$

The radiative lifetime $\tau_r(\Psi J)$ of an excited level $(\Psi J)$ is equal to the reciprocal of $A_t(\Psi J)$ [19].

$$\tau_r(\Psi J) = \frac{1}{A_t(\Psi J)} \quad (12)$$

The $\beta_r$, $A_{rad}$, $\tau_r$, $\tau_{exp}$ and η for the $^4I_{13/2} \rightarrow {}^4I_{15/2}$ transitions of Er⁺³ ions in PANKB0.2Er, PANKB0.75Er, PANKB1.5Er and PANKB3Er glasses are tabulated with experimental lifetime ($\tau_{exp}$) and quantum efficiency (η) in Table 6.

*Mc-Cumber Model.*

The absorption cross-section $(\sigma_a)$ can be calculated from absorbance data using equation (13)

$$\sigma_a = 2.302 \frac{A}{NL} \quad (13)$$

Where A is the absorbance, *N* is the Er⁺³ ions concentration per cubic cm and L is the sample thickness.

Mc-Cumber equation [20] relates absorption and emission cross-section as follows:-

$$\sigma e(\nu) = \sigma a(\nu) e^{(\varepsilon - h\nu)/K_B T} \quad (14)$$

Where $\varepsilon$ is as the net free energy required for exciting one Er³⁺ ion from the $^4I_{15/2}$ to the $^4I_{13/2}$ state at temperature *T*. The absorption cross-section ($\sigma_a$) has been calculated by equation (13) as previously reported in [21].

Fig. 5 shows the $\sigma_a$ (black line) and the $\sigma_e$ (red

**TABLE 3. Judd–Ofelt parameters ($\Omega_t$ x $10^{-20}$ cm$^2$) for PANKB0.2Er, PANKB0.75Er and PANKB1.5Er glasses**

| HOST MATRIX | $\Omega_2$ | $\Omega_4$ | $\Omega_6$ | Trend |
|---|---|---|---|---|
| PANKB0.2Er | 2.16 | 0.34 | 0.49 | $\Omega_2 > \Omega_6 > \Omega_4$ |
| PANKB0.75Er | 0.6 | 0.31 | 0.36 | $\Omega_2 > \Omega_6 > \Omega_4$ |
| PANKB1.5Er | 0.5 | 0.36 | 0.4 | $\Omega_2 > \Omega_6 > \Omega_4$ |
| PANKB3Er | 0.91 | 0.37 | 0.44 | $\Omega_2 > \Omega_6 > \Omega_4$ |

line) for PANKB3Er glass as a representative data. It can be noticed that at longer wavelengths, $\sigma_e$ is higher than $\sigma_a$ while for shorter wavelengths, $\sigma_e$ is smaller than $\sigma_a$. This phenomenon may be attributed to that the manifold splitting for rare earth ions in crystal or glass matrices is several hundred cm$^{-1}$, larger than the value of KT. Table 4 shows the peak position and peak value of $\sigma_a$ and $\sigma_e$ for the prepared samples.

*The internal gain factor G*

The internal gain factor (*G*) as a function of wavelength $\lambda$ can be calculated by equation (15).

$$G(\lambda) = \sigma_e(\lambda)N_2 - \sigma_a(\lambda)N_1 \qquad (15)$$

Where $N_1$ and $N_2$ are the concentration of ions in the ground and excited state, respectively and $N_1 + N_2 = N$ where N is the total concentration of erbium ions [22]. The population inversion rate can be given by equation (16).

$$P = \frac{N_2}{N} \qquad (16)$$

Fig. 6 shows the gain spectra as a function of wavelength at different population inversion rate (P = 0, 0.2, 0.4, 0.6, 0.8 and 1) for PANKB3Er as a representative data. When *G* has a positive value it mean that there is an amplification process. When *G* has a negative value it means that there is a loss or attenuation in the signal. The change in population inversion rate strongly modifies the internal gain coefficient of the glass. For *P* = 0 the gain coefficient have a negative value for the full range. For low values of the population inversion, the glass is like an absorber of the light for the shorter wavelengths, while it amplifies at longer wavelengths. By increasing *P* the positive region of *G* increased and the negative region decreased. For *P* = 1 the gain is completely positive and has the maximum value of amplification.

Table 5 shows *G* and the wavelength of maximum gain ($\lambda_m$) at different *P* values. one can notice that there is a positive gain value for

low population inversion rate (only 0.2) at longer wavelengths and this is due to that $\sigma_e$ is larger than $\sigma_a$ at longer wavelengths. By increasing the value of *P*, $\lambda_m$ shifts toward shorter wavelengths for all samples. This is can be explained by looking at gain equation (15) where by increasing the value of *P*, $N_1$ decreases hence, the effect of the absorption process decreases.

*Fluorescence Spectra*

Fig. 7 shows the near IR emission spectra of PANKB1.5Er and PANKB0.75Er glasses as representative samples. The Er$^{3+}$ ions firstly excited to $^2H_{11/2}$ using a diode laser (514.5nm). The $^2H_{11/2}$ then relaxes radiatively and non-radiatively to $^4I_{13/2}$ level which, radiatively relaxes to the ground state and emitting the characteristic band around 1536 nm. The emission intensity found to be linearly increase with increasing the Er$^{3+}$ concentration which indicating that physical clustering is practically negligible. The inset shows the same graphs in normalized scale and it can be obviously seen that the IR emission band profiles aren't modified by the Er$^{3+}$ ions concentration. The position and shape of the bands are the same for all samples which indicating that the Er$^{3+}$ ions are homogeneously distributed within the glass matrix and there is no variation in the local field around Er$^{3+}$ ions.

Fig. 8 shows the normalized emission decay curve of $^4I_{13/2}$ level for the PANKB1.5Er and PANKB0.75Er glasses in semi-lograthmic scale. As obviously seen, the entire samples show a non-single exponential decay curve profile for IR emission. The experimental lifetimes, were calculated at 1/e of intensity at t=0. The experimental lifetimes are tabulated with other radiative properties in Table 6.

The spectroscopic radiative properties of the $^4I_{13/2} \rightarrow ^4I_{15/2}$ transition are presented in Table 6 for all prepared samples.
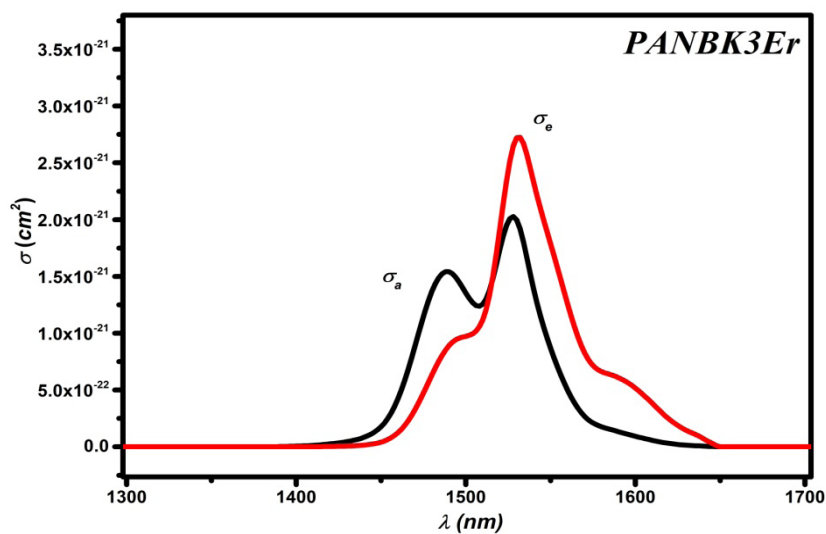
**Fig. 5. The σ_a (black line) and the σ_e (red line) for PANKB3Er glass.**

**TABLE 4. The peak position and peak value of σ_a and σ_e for the prepared samples.**

| Samples | σ_a | | σ_e | |
|---------|---------------|------------|---------------|------------|
| | Peak position | Peak value | Peak position | Peak value |
| PANKB0.2Er | 1528 | 2.05 | 1532 | 3.1 |
| PANKB0.75Er | 1522 | 1.82 | 1524 | 2.42 |
| PANKB1.5Er | 1522 | 1.92 | 1524 | 2.45 |
| PANKB3Er | 1528 | 2.02 | 1532 | 2.83 |



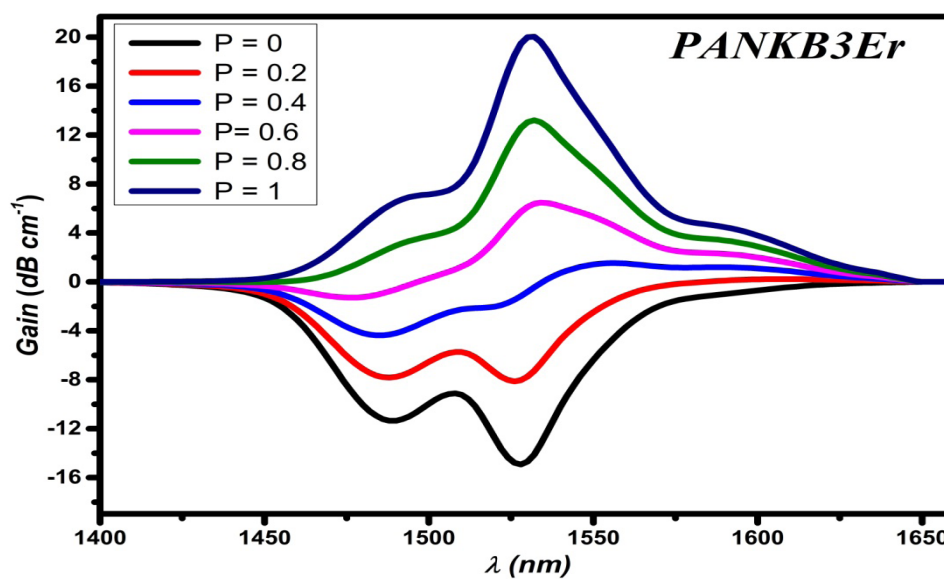**Fig. 6. Gain spectra as a function of wavelength at different values of inversion population rate (P = 0, 0.2, 0.4, 0.6, 0.8 and 1) for PANKB3Er glasses.**
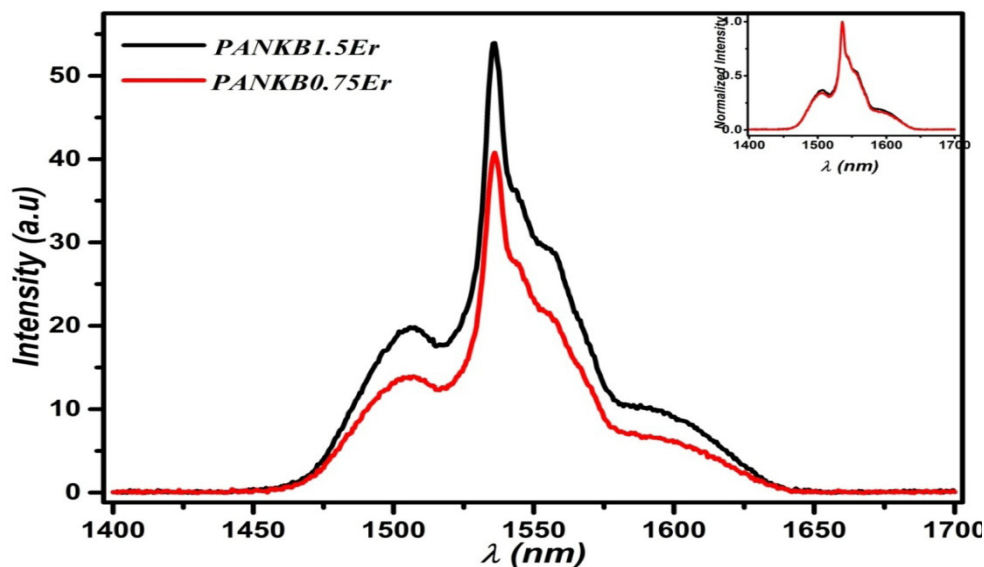
**Fig. 7.The fluorescence spectrum of PANBK1.5Er,and PANBK0.75Er glasses (excitation with 514.5 nm), the inset shows the same graphs in normalized scale.**
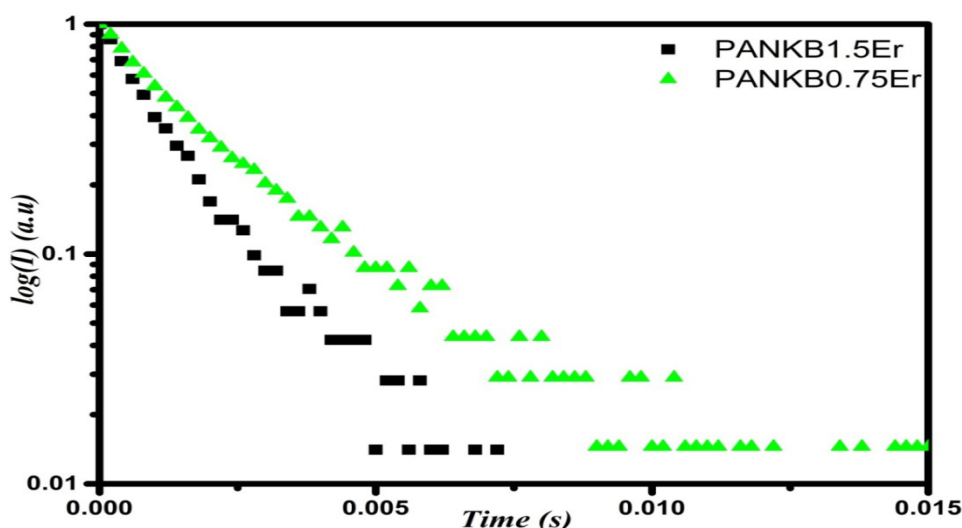


**Fig. 8. The emission decay curve of 4I13/2 level for the PANBK1.5Er and PANBK0.75Er glasses, in semi-logarithmic scale.**

**TABLE 6 the prepared samples branching ratio ($B_R$), total transition probability ($A_T$), radiative lifetime ($\tau_r$), experimental lifetime ($\tau_{exp}$) and quantum efficiency ($\eta$) for the $^4I_{13/2} \rightarrow ^4I_{15/2}$ transition.**

| Series | Glass Samples | Parameters | | | | |
|---|---|---|---|---|---|---|
| | | $B_r$ | $A_t (s^{-1})$ | $\tau_r$ (ms) | $\tau_{exp}$ (ms) | $\eta$ |
| | PANKB0.2Er | 1 | 97.1 | 10.29 | - | - |
| | PANKB0.75Er | 1 | 83.73 | 11.94 | 1.8 | 15.01% |
| | PANKB1.5Er | 1 | 86.15 | 11.48 | 1.2 | 10.45 |
| | PANKB3Er | 1 | 90.03 | 11.11 | - | - |

**TABLE 5. The G and peak maximum $\lambda_p$ at different P values for series the prepared samples.**

| Sample | P | G | $\lambda_m$ |
|---|---|---|---|
| | 0.2 | 0.01 | 1594 |
| PANKB0.2Er | 0.6 | 0.4 | 1532 |
| | 1 | 1.3 | 1530 |
| | 0.2 | 0.03 | 1592 |
| PANKB0.75Er | 0.6 | 1.42 | 1524 |
| | 1 | 4.54 | 1522 |
| | 0.2 | 0.06 | 1594 |
| PANKB1.5Er | 0.6 | 2.75 | 1524 |
| | 1 | 9.1 | 1522 |
| | 0.2 | 0.02 | 1608 |
| PANKB3Er | 0.6 | 6.48 | 1534 |
| | 1 | 20.8 | 1532 |

The $\tau_r$ has a maximum value of 11.94 for PANKB0.75Er sample. The $A_t$ has an opposite trend to $\tau_r$. The $\tau_{exp}$ decreased by increasing the $Er^{3+}$ ions content and it have a maximum value equal to 1.8 ms. The decrease in lifetimes is attributed to an increase in non-radiative processes. $\eta$ was found to be decreased with increasing of $Er^{3+}$ ions content and it has a maximum value equal to 15.01% for PANKB0.75Er glass. The $B_r$ has a constant value for all samples.

## Conclusion

Er3+doped Na-Al-K-Ba phosphate glasses prepared by conventional melt quenching technique. The XRD patterns show that all the samples were in an amorphous form. The density and refractive index were measured and it is almost constant for different Er3+ ions concentration. The dielectric measurements show that the samples have a higher $\sigma_{ac}$ value at 3 mol % of $Er^{3+}$ ions concentration due to the increase in charge carriers as confirmed from the obtained ρ data.

The absorption spectra were measured and analyzed using the Judd-Ofelt model. High radiative and experimental lifetime for the $Er^{3+}$ ions has been noticed. The experimental lifetime and quantum efficiency found to be decreased with increasing in $Er^{3+}$ions content which is attributed to an increase in non-radiative processes. These results obviously indicate that present glasses are promising for laser and optical amplifiers around 1.5 μm.

## References

1. Yamada M, Ono H, Kanamori T, and Ohishi Y, Broadband and gain flattened amplifier composed of a 1.55 μm-band and 1.58 μm-band $Er^{+3}$ - doped fiber amplifier in a parallel configuration *Electron Lett*, 33 710-711(1997).

2. Ohishi Y, Mori A, Yamada M, Ono H, Nishida Y, and Oikawa K, Gain characteristics of tellurite-based erbium-doped fiber amplifiers for 1.5-μm broadband amplification. *Optics Letters*, 23 274-276(1998).

3. Lira A, Camarillo C I, Camarillo E, Ramos F, Flores M, and Caldino U, Spectroscopic characterization of $Er^{3+}$ transitions in $Bi_4Si_3O_{12}$. *J. Phys.: Condens. Matter*, 16 5925-5936(2004).

4. Yamane M and Asahara Y, Glasses for Photonics. 2004: Cambridge University Press.

5. Digonett M J, *Rare-Earth-Doped Fiber Laser and Amplifier*. 2001: Marcel Dekker, Inc.

6. Ismail M M, Farouk H, Salem M A, Ashery A, and Battisha I K, Optical properties of $Er^{3+}$ doped phosphate glasses. *Journal of Scientific Research in Science*, 36(1), 469-483(2019).

7. Xu X and Day D E, Properties and structure of Sn-P-O-F glasses. (1990).

8. Rocha M S F, Pontuschka W M, and Blak A R, *Non-Cryst. Solids*, 321 29(2003).

9. Babu P, Seo H J, Jang K H, Balakrishnaiah R, Jayasankar C K, Lim K-S, Lavín V, and Optical spectroscopy μ e, and upconversion properties

of Er³⁺-doped metaphosphate laser glasses, J. Opt. Soc. Am. B 24 (2007) 2218–2228., Optical spectroscopy, 1.5 μm emission, and upconversion properties of Er³⁺-doped metaphosphate laser glasses. *J. Opt. Soc. Am. B*, 24 2218-2228(2007).

10. Santos C C, Guedes I, Loong C K, Boatner L A, Moura A L, Araujo M T d, Jacinto C, and Vermelho M V D, Spectroscopic properties of Er³⁺-doped lead phosphate glasses for photonic application. *Physics D: Applied Physics*, 43(2), 025102(2009).

11. Reddy A A, Babu S S, Pradeesh K, Otton C J, and Prakash G V, Optical properties of highly Er³⁺-doped sodium–aluminium–phosphate glasses for broadband 1.5 μm emission. *J. Alloy. Compd*, 509 4047-4052(2011).

12. Luewarasirikula N, Chanthimab N, Tariwongb Y, and Kaewkhaob J, Erbium-doped calcium barium phosphate glasses for 1.54 μm broadband optical amplifier *Materials Today: Proceedings*, 5 14009–14016(2018).

13. RELIC. Available from: https://www.lanl.gov/ projects/feynman-center/deploying-innovation/ intellectual-property/software-tools/relic/index. php.

14. Judd B R, Optical absorption intensities of rare earth ions. *Phys. Rev*, 127 750(1962).

15. Ofelt G S, Intensities of Crystal Spectra of Rare-Earth Ions. *Chemical Physics*, 37 511-520(1962).

16. Mohan S, Thind K S, and Sharma G, Effect of Nd³⁺ concentration on the physical and absorption properties of sodium-lead-borate glasses. *Brazilian Journal of Physics*, 37 1306-1313(2007).

17. P.Hehlen M, MikhailG.Brik, and KarlW.Krämer, 0th anniversary of the Judd–Ofelt theory: An experimentalist's view of the formalism and its application. *Journal of Luminescence*, 5136 221-239(2013).

18. Jorgensen C K and Reisfeld R, Judd–Ofelt parameters and chemical bonding. *Less-Common Met.*, 93 107(1983).

19. Weber M J, Probabilities for Radiative and Nonradiative Decay of Er³⁺ in LaF₃. *PHYSICAL REVIEW*, 157(2), 262-272(1967).

20. McCumber D E, Einstein Relations Connecting Broadband Emission and Absorytion Syectra. *PHYSICAL REVIEW*, 134 A954-A957(1964).

21. Miniscalco W J and Quimby R S, General procedure for the analysis of Er³⁺ cross sections. *Optics Letters* 16 258-260(1991).

22. Desurvire E, *Erbium-Doped Fiber Amplifiers, Principles and Applications*. 1994, New York: John Wiley.

23. A. Jonscher, *Thin Sol Films* 100, 329 (1983). https://doi.org/10.1016/0040-6090(83)90157-8.